VIRGINIA TECH

USE OF THE TRAFFIC SPEED DEFLECTOMETER FOR THE STRUCTURAL ASSESSMENT OF CONCRETE PAVEMENTS

TPF-5(385) Pavement Structural Evaluation with Traffic Speed Deflection Devices

TASK 4: DEMONSTRATE HOW STRUCTURAL CONDITION COLLECTED FROM TSDDS CAN BE USED FOR SUPPORTING PROJECT LEVEL DECISION-MAKING

AUTHORS: MARTIN SCAVONE, EUGENE AMARH, SAMER KATICHA, GERARDO FLINTSCH

SUBMITTED: AUGUST 2023

VIRGINIA TECH TRANSPORTATION INSTITUTE
VIRGINIA TECH
Center for Sustainable and Resilient Infrastructure

Use of the Traffic Speed Deflectometer for the Structural Assessment of Jointed Concrete Pavements

TABLE OF CONTENTS

CHAPTER 1. Introduction

1.1. Purpose and Scope

The purpose of this document is to summarize recent progress in the analysis and interpretation of Traffic Speed Deflectometer (TSD) data collected on jointed concrete pavements. Historically, most TSD-related research focused on the analysis and interpretation of deflection slope or deflection basin estimates collected from measurements on flexible pavements. Use of the TSD for the structural assessment of jointed pavements (either plain concrete pavements or composites) has been very limited. The TSD is regarded as capable of detecting spots with localized structural deficiencies (Phares et al., 2008; Flintsch et al., 2013; Katicha et al., 2014 and 2017), such as the weakest joints in a jointed pavement segment, yet no major progress concerning the interpretation of the TSD data after detecting those weak spots has been published. Furthermore, the only published standard on TSD operation (Austroads, 2016) advises against TSD surveying on rigid pavements (concrete and composites).

The release of the fourth generation TSD in 2020, with enhanced sensing capabilities compared to the previous TSD versions and able to report deflection data with a spatial resolution as low as 2 inches [5 cm], re-ignited the interest in concrete pavement deflection surveying. After a trial run with the TSD on jointed concrete segments in Europe (Nielsen et al., 2023) and another in the United States (Scavone et al., 2022; 2023) data interpretation methods were proposed to estimate the concrete pavement's strength parameters and the joints' *Load Transfer Efficiency* index (LTE) from the TSD data (Nielsen et al., 2023; Scavone et al., 2023; Hernandez, 2023 – in press). This report provides a review of one of these techniques developed as part of the TPF-5(385) research activities, whose software implementation has been publicly released *open source*[1]*).*

1.2. Audience

This report's target audience is any practitioner or researcher on TSD technology.

[1]The computer source code to the LTE back-calculation procedure is publicly available (under the CC BY-SA 4.0 International License terms) in https://github.com/MartinScavone/concreteTSD

CHAPTER 2. TSD Deflection Velocity Data

2.1. Introduction

The TSD's pavement surface deflection sensing system consists of an array of Doppler Laser Vibrometers (Hildebrand and Rasmussen 2002, Katicha et al., 2021) that measure the velocity at a point on the pavement surface at a given distance from the TSD rear axle wheel. The Doppler Effect is the physical principle behind the TSD's relative velocity measurements (Jendzurski and Paulter, 2008).

The earliest TSD devices featured 3 Doppler vibrometers pointed at locations within the rear axle deflection basin, plus a *reference sensor* far away from the axle that measures the pavement velocity at an undeflected location. The second-generation TSDs (Austroads 2016) carry seven sensors, and the third- and fourth-generation TSDs carry 10 or 11 sensors, apart from the *reference sensor.*

The Doppler Effect is the shift in wave frequency that is observed after an emitted wave returns to the source after being reflected by an object that is moving relative to the wave source. The relative velocity between the wave source and the object that produces the reflection is directly related to the amount of shift in the wave frequencyas follows:

$$\begin{gathered}\text{source and receiver approaching:} \\ f_{perceived} = \frac{c}{c - v \times cos(\theta)} f_0 \\ \text{source and receiver departing:} \\ f_{perceived} = \frac{c}{c + v \times cos(\theta)} f_0\end{gathered} \tag{1}$$

In equation 1, f_0 is the frequency of the emitted wave, $f_{perceived}$ is the frequency of the reflected wave, c denotes the waves' propagation speed for the medium the wave was emitted in, v is the relative velocity between the wave source and the object where the reflected wave is produced, and θ represents the angle between the vector v and the direction at which the wave is propagating (Jendzurski and Paulter, 2008). In the familiar case of a driving speed radar (Jendzurski and Paulter, 2008), waves are emitted from a static source (the radar), and the speed of incoming vehicles is estimated from the shifted frequency of these waves' reflections. The radar would estimate the component of the vehicle's speed v that is collinear with the radar's beam. The measured velocity component, *M,* would be:

$$M = v \times cos(\theta) \tag{2}$$

Where theta is the angle between the vehicle's velocity vector and the vehicle-radar line – Figure 1.

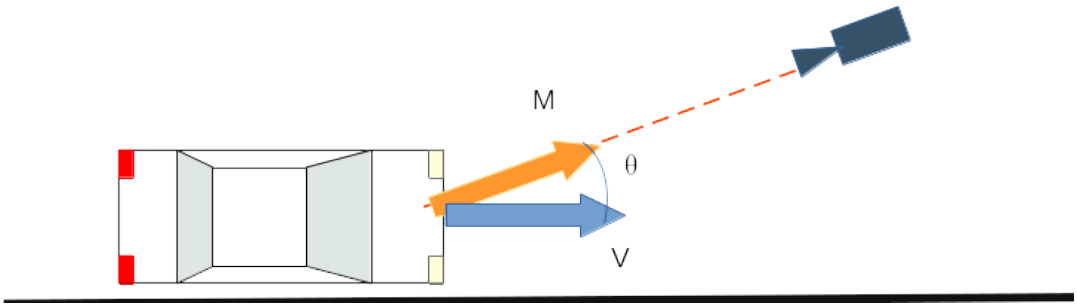

Figure 1: Example of speed-check radar measurement.

The Doppler laser sensors mounted on the TSD measure the relative velocity between the device and the pavement surface – both the wave source, which is the Doppler laser in the TSD, and the pavement surface where the reflection is generated are in motion. In this case, the Doppler lasers' relative velocity measurement (that is, a velocity measurement relative to the Doppler sensor) has both a horizontal component (TSD travel speed v_x) and a vertical component (the pavement surface's deflection velocity – v_y). This concept is illustrated in Figure 2 (see Appendix 1 for more details).

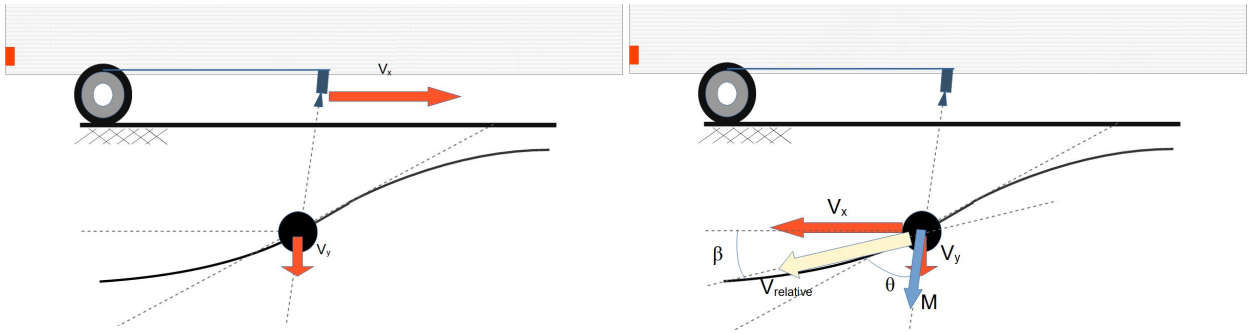

Figure 2: Concept illustration of pavement v_y measurement with a TSD. Left: pavement's v_y and TSD's v_x from an *outside* point of view. Right: Pavement's relative velocity with respect to a TSD-based point of view. The TSD sensor's measurement M, a projection of $V_{relative}$ over the sensor's beam direction is also shown.

2.2. V_y and deflection slope

Traditionally, the pavement's v_y measurements from the multiple Doppler sensors are converted to *deflection basin slope* measurements following the expression given in equation 3 (Krarup et al., 2006; Katicha et al. 2021).

$$S(r) = \frac{v_y(r)}{v_x} \tag{3}$$

Where $S(r)$ is the slope of the deflection basin at a distance r from the TSD's rear axle, $v_y(r)$ is the deflection velocity measurement for the Doppler sensor located in position r, and v_x is the TSD's travel speed. These deflection slope estimates are integrated over the TSD's longitudinal direction to obtain the deflection basin up to a constant of integration (Krarup et al., 2006; Müller and Roberts, 2012; Flintsch et al., 2013; Katicha et al., 2021). Alternatively, deflection indices (Horak.,

2008) can be computed directly from these deflection slope estimates (Rada et al., 2016; Katicha et al., 2021).

However, Scavone et al. (2022) showed that equation 3 only holds under the assumption that the deflection basin in response to the moving TSD load is *stationary* – it does not change shape as the TSD moves along the pavement. This can be proved using the *chain rule* of derivatives and the concept of *total* and *partial derivatives.* Using the chain rule, the relationship between v_y (the total derivative of the deflection function for a fixed point on the pavement surface, measured by the TSD at a given instant) and the deflection basin slope (a *local* derivative of a traveling deflection basin) is given in equation 4:

$$v_y(r) = S(r) \times v_x + \frac{\partial w^*}{\partial t}(r) \tag{4}$$

In which v_y, v_x, and *S(r)* are the same as for equation 3, and the *partial derivative term* $\partial w^*/\partial t$ represents how much the deflection basin, at a distance *r* from the load center, changes shape – any discontinuity in the pavement structure, such as open joints or cracks, or changes in layer thicknesses or material properties would make the *partial derivative term* non-zero.

More details into the v_y – slope relationship, and the mathematical derivation of equation 4 is given in Appendix 2.

2.3. V_y from a jointed pavement

Jointed pavements are one important case where equation 3 does not hold and the extra term in the chain rule (Equation 4) cannot neglected: The transverse joint, a discontinuity in the pavement structure, makes the traveling deflection basin changes shape (Figure 3), and therefore, the *partial derivative term* in a TSD's v_y signal equation 4 is non-zero (Figure 4) **(**Scavone et al., 2022)[2]. The difference between v_y and *S* can be illustrated qualitatively in Figure 4: As the TSD load approaches the joint, *S* changes sign because of the change of shape in the deflection basin However, the points on the pavement surface, ahead of the TSD whee,l (like the locations usually *sensed* by the TSD) are moving downward at all times, which means that v_y does not change sign. This shows that the slope, *S*, and v_y do not have the same sign and therefore, the slope, is not equal to v_y/v_x. This shows that the deflection velocity, not the deflection slope, should be used when analyzing TSD measurements on jointed pavements.

[2]Note: The deflection basins and v_y signal shown in figures 2 and 3, reproduced from Scavone et al., (2022), were simulated using linear-elastic slab theory (Van Cauwelaert, 2004). This mathematical framework was found to represent satisfactorily the response of a jointed pavement to a rolling axle load like that of a TSD and match the outcome of a finite element model without the incurred computational cost (Deep et al., 2020). Scavone et al. (2022) provided the additional step to simulate the TSD's v_y measurements and deflection slope signals for a jointed pavement by appealing to this framework.

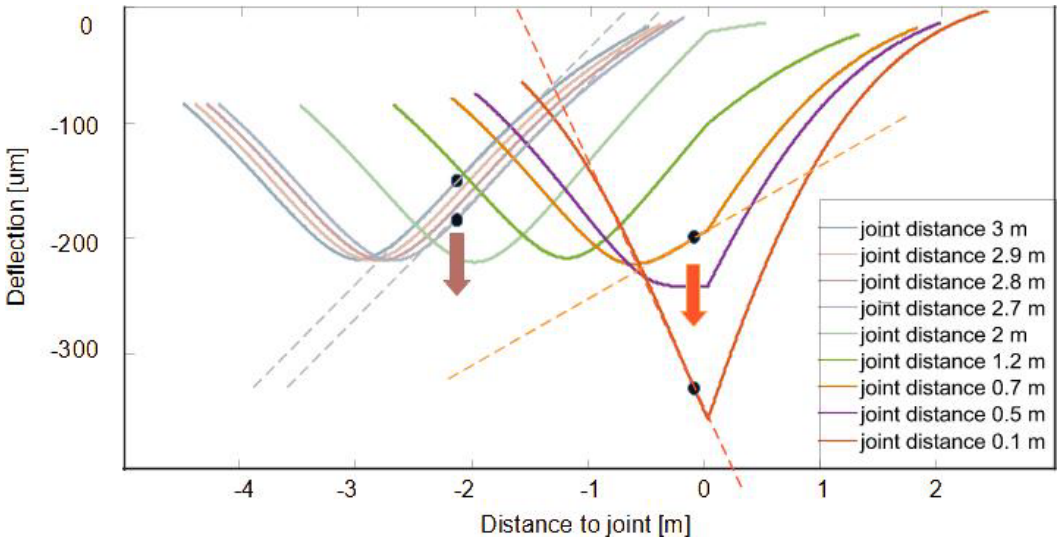

Figure 3: Simulated deflection bowls for a TSD/ load approaching a transverse joint (at x = 0). The arrows indicate the direction of v_y for points ahead of the load, whereas the dotted straight lines follow their deflection slope (Scavone et al., 2022).

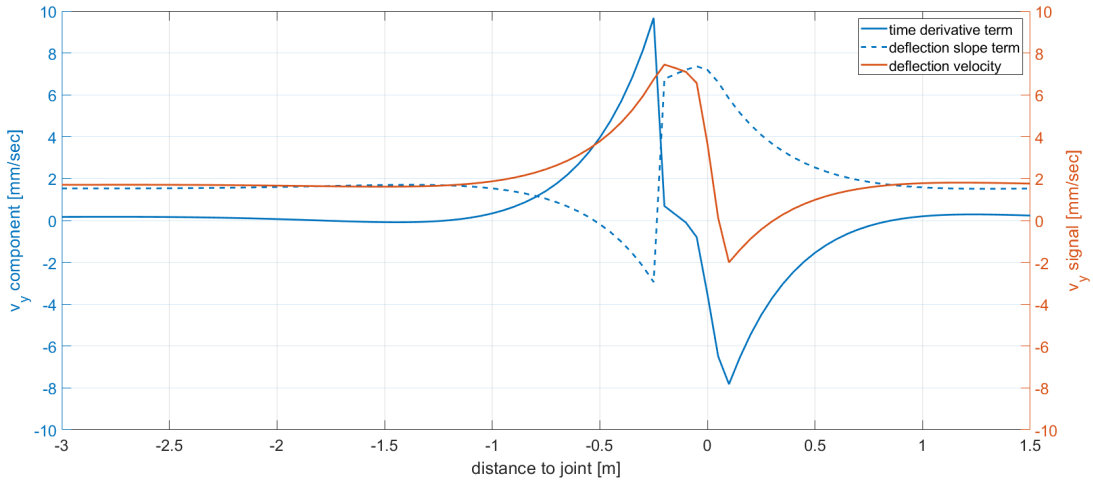

Figure 4: Simulated TSD v_y [red] and deflection slope [blue dotted] signals for a pavement with a transverse joint (located at x = 0). The partial derivative term (equation 4) is non-zero nearby the joint. (Scavone et al., 2022)

Scavone et al. (2022) also showed that the TSD v_y measurements for a jointed concrete pavement can be replicated with a linear-elastic slab-on-ground model (Van Cauwelaert, 2004). Following is an example from the MnROAD *Load Volume Road* (Figure 5). TSD v_y measurements were collected at a 5-cm spatial resolution (spacing between consecutive measurements) in September 2021. This measurement campaign included three jointed concrete sections built in 2017, whose thickness and material properties are reported (Van Deusen et al., 2018; Barman et al., 2021; Khazanovich et al., 2021). Figure 5 shows a sample of the TSD's v_y data for one of the three concrete sections, for which the joint spacing is 6 feet. The pulses in the v_y signal represent the passage of the TSD wheel over the transverse joints. A simulated v_y signal resembling the TSD data for a single transverse joint was overlaid to the data with a reasonable match, demonstrating

that by fine-tuning Van Cauwelaert's (2004) slab-on-ground model parameters (explained in detail in **Appendix 3)**, the TSD measurements can be replicated and, consequently, the pavement properties and the joint's LTE index can be backcalculated from TSD measurements.

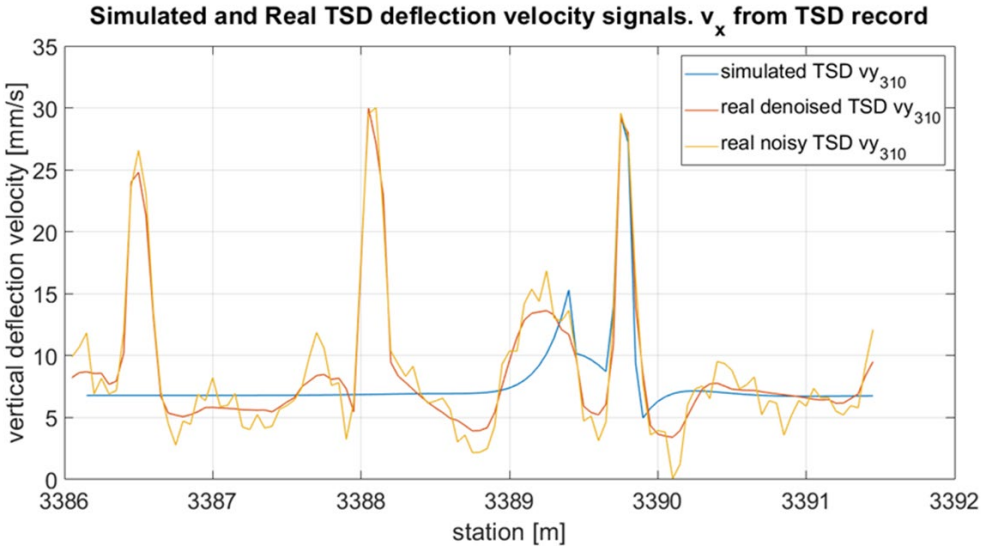

Figure 5: Measured TSD v_y signal (+310mm sensor) for a jointed pavement and a matched simulated v_y pulse for a single joint.

CHAPTER 3. Back-calculation of concrete pavement properties from TSD v_y data

3.1. Introduction

This chapter discusses two possible approaches to back-calculate the structural properties of a jointed concrete pavement from TSD measurements. One approach consists of implementing the concept of *v_y profile matching* introduced in Figure 5 (matching modeled v_y signals to measurements from a single sensor of the TSD collected as the TSD rolled over the joint) while the other approach (Scavone et al., 2023) performs back-calculation of the *v_y basins*, like the back-calculation procedure based on deflection basin depth data proposed for the Falling Weight Deflectometer (FWD) (Rohde et al., 1991; Ullidtz, 1987; and Schmalzer et al., 2007).

The collection of v_y measurements collected by the many sensors of the TSD along a pavement segment can be regarded as a two-dimensional v_y array (Figure 6). **Throughout this chapter, a collection of v_y measurements from a single joint will be referred to as *v_y profile,* whereas the set of measurements from all sensors gathered at a single location will be called *v_y basin.***

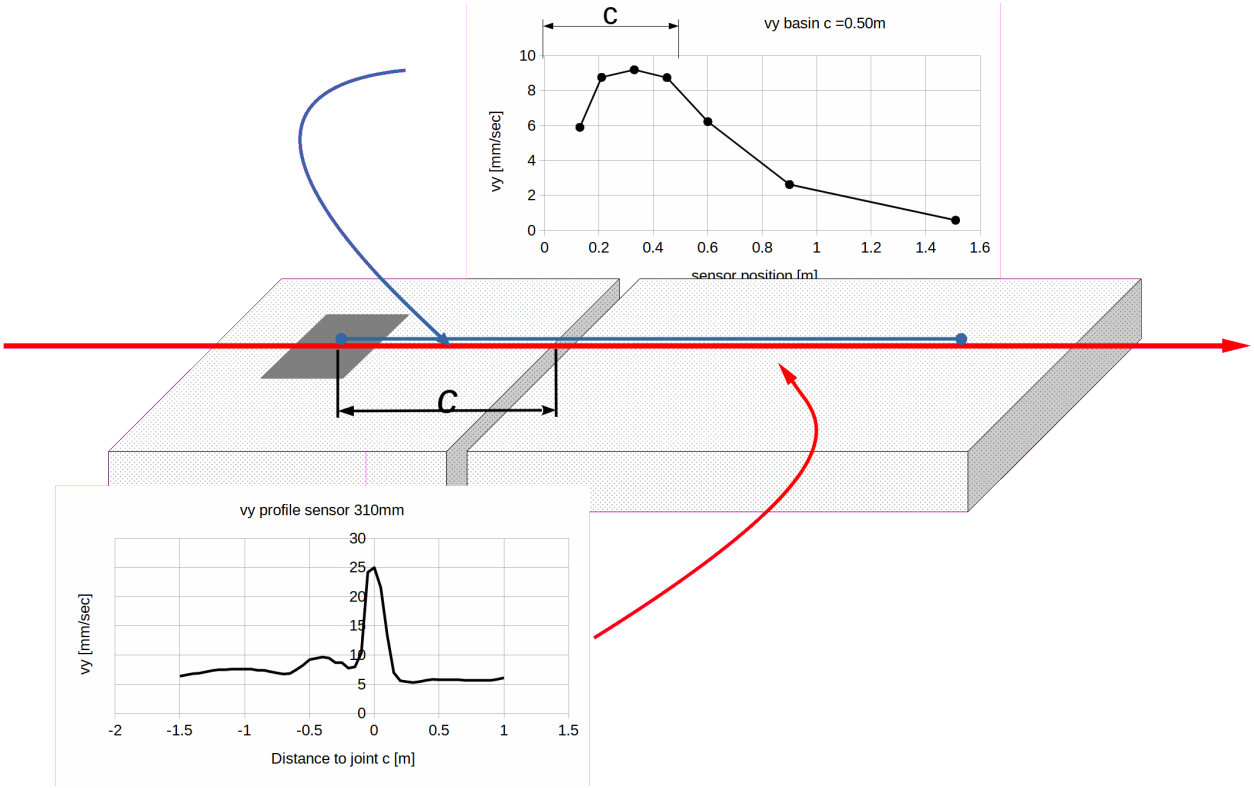

Figure 6: Example of v_y basin (multiple sensor measurements for a single station – blue) and v_y profile for a single sensor (red)

Two analysis methodologies were developed to interpret the TSD's v_y data and back-calculate the pavement properties and the joint's LTE index

For the two methodologies, the concrete parameter estimation problem is reduced to an optimization problem whose objective is to minimize a metric of the error between the modeled response $\boldsymbol{w}$ and the measured TSD data by manipulating the pavement model's parameters

(summarized as vector $\boldsymbol{\theta}$ in equation 5). Both procedures rely on Van Cauwelaert's (2004) linear elastic slab-on-ground model **(Appendix 3)** to simulate the pavement response that is to be matched to the selected set of TSD measurements and in both cases it is assumed that the concrete slab thickness and Poisson's coefficient is known, thus vector $\boldsymbol{\theta}$, the variable to solve for contains the concrete slab's elastic modulus E, the subgrade's modulus of reaction k and modulus of shear strength per unit length $\boldsymbol{G}$, and the joint's Load Transfer Efficiency index [LTE].

$$\begin{gathered} \min_{\theta} \; f(\|TSD_{data} - w(\theta)\|) \\ \text{where:} \quad \theta = [LTE, E, k, G] \\ \text{assuming: } h, \nu \text{ known} \end{gathered} \tag{5}$$

However, as discussed in Chapter 2, the implementation of equation 5 within a TSD analysis framework must be based on v_y data therefore, the function w(θ) actually is deflection velocities.

3.2. Back-calculation of concrete pavement properties based on v_y basins.

This procedure is an adaptation of the well-known back-calculation problem from deflection data as formulated by Rohde and Smith (1991): Deflection data from multiple sensors collected at a given location within the pavement (a deflection basin for the FWD, and a v_y *basin* for the TSD) are compared to the modeled response for the sensors' locations and a given set of values for the model parameters (vector θ), the sum of squared errors (SSE) between measurements and modeled responses is computed. The back-calculation problem consists of determining the value of $\boldsymbol{\theta}$ that minimizes SSE.

For the case of the TSD, the measurements used are the deflection velocities and therefore, the SSE must be stated in terms of deflection velocities [v_y] (Scavone et al., 2023 – in press). The TSD back-calculation problem is stated in equation 6.

$$\begin{gathered} \min_{\theta} \|TSD - \dot{w}(\theta)\|^2 = \sum_{i=1}^{TSD-sensors} \left(TSD_i - \dot{w}_i(\theta)\right)^2 \\ \text{where:} \quad \theta = [LTE, E, k, G] \\ \text{and:} \quad \dot{w}_i(\theta) = v_y(x_{TSDi}, \theta) \\ \text{subject to: } E > 0, k > 0, G > 0, LTE \in [0,1] \\ \text{assuming: } h, \nu \text{ known} \end{gathered} \tag{6}$$

In equation 6, x_{TSDi} represents the distance between the TSD's rear axle wheel and the i-th sensor, the coordinate x is moving with the TSD wheel.

Scavone et al. (2023) implemented a numerical solution to the problem in equation 6 that divides the back-calculation problem into two subproblems. The first determines the pavement properties from the data collected mid-slab and the second determines the joint strength properties from data collected near the joints. This is similar to the two-stage back-calculation of concrete pavements from FWD data proposed by Ullidtz (1987):

- Optimization Problem 1 [OP1]: Use mid-slab v_y measurements to fit an infinite slab model (ignore the presence of the joint). Solve for the pavement and subgrade's strength parameters.

- Optimization Problem 2 [OP2]: Assuming the results from OP1 [*E, k, G*] as valid, fit the jointed slab-on-ground model to solve for the joint's LTE index. Scavone et al. (2023) also proposed OP2 as a refinement to the distance between the TSD wheel and the joint *c.*

Mathematically, problems OP1 and OP2 are stated as follows (equation 7):

$$
\begin{array}{cc}
OP1: min_{\ \theta} \sum_{i=1}^{TSD-sensors} \left(TSD_{midslab_i} - \dot{w}_i(\theta)\right)^2 & OP2: min_{\theta} \sum_{i=1}^{TSD-sensors} \left(TSD_{joint_i} - \dot{w}_i(\theta)\right)^2 \\
\text{where: } \dot{w}_i = v_y(x_{TSDi}, \theta) & \text{where: } \dot{w}_i = v_y(x_{TSDi}, \theta) \\
w(x,\theta) \text{ from infinite slab defl. model,} & \text{and: } w(x,\theta) \text{ from jointed slab defl. model} \\
\text{and: } \theta = [k, E, G] & \text{and: } \theta = [c, LTE] \\
\text{Subject to: } k \geq 0, E \geq 0, G \geq 0, & \text{Subject to: } c_{min} \leq c \leq c_{max},\ 0 \leq LTE \leq 1, \\
\text{assuming: } h, \nu \text{ known} & \text{assuming: } h, \nu, k, E, G \text{ known}
\end{array}
\tag{7}
$$

Scavone et al. (2023) implemented the *two-stage* concrete back-calculation problem (equation 7 and) onto computer code to process 5-cm-resolution TSD measurements from concrete pavements with regular-size (15-20 feet long) slabs:

- Firstly, the TSD data is denoised and the pulses recorded as the TSD travels over the joints are located.
- Then, for every joint detected:
  - Problem OP1 is solved for the mid-slab measurements recorded between 68 and 88 inches [2.25 and 1.75 meters] ahead of the pulse location. The mean of the multiple *k, E,* and *G* are recorded as the local pavement properties.
  - Problem OP2 is solved for all the measurements recorded between 59 and 8 inches [1.50 to 0.20 meters] ahead of the joint. The mean LTE from each instance is reported as the joint's final LTE estimate.

3.3. Back-calculation of concrete pavement properties by matching of v_y profiles.

An alternative concrete pavement back-calculation procedure for TSD data consists of analyzing the v_y profiles collected by a single sensor at multiple locations near a transverse joint; the amplitude and shape of the measured v_y profile contains information about the pavement's structural capacity and the joint's LTE index (Scavone et al., 2022). Therefore, matching the measured v_y*-profile* to the modeled v_y*-profile* allows the determination of pavement structural parameters and the joint's LTE

Mathematically, the v_y *profile matching* problem can be stated as an optimization problem. For example, in the case of a TSD survey on a pavement with known slab thickness *h* and concrete's Poisson's coefficient ν, and unknown concrete modulus *E,* soil properties *k,* ***G***, and joint LTE, the correlation between measured v_y data and modeled v_y profiles can be set as the *objective function* (the function to optimize). More specifically, the correlation between the normalized measurements and modeled responses is set as the optimization objective function, so that v_y*-matcher* would be insensitive to systematic measurement errors (bias) that would otherwise distort the results. Conceptually, this formulation is focused on matching the *shape* of the v_y data rather than its mere numerical values. V_y*-matcher*'s mathematical formulation is stated below (equation 8).

$$
\begin{gathered}
max_{\theta} corr(X(\theta), Y) \\
\text{where } \theta = [E, k, LTE | \nu, Load, h, v_x, G = 0] \\
and: corr(X,Y) = \frac{cov(X,Y)}{\sigma_X \times \sigma_Y} = \frac{E[(X-\mu_X)(Y-\mu_Y)]}{\sigma_X \times \sigma_Y} \\
in\ which:\ X = = \frac{v_y - \mu_{v_y}}{\left\| v_y - \mu_{v_y} \right\|};\quad Y = \frac{TSD - \mu_{TSD}}{\|TSD - \mu_{TSD}\|}
\end{gathered}
\tag{8}
$$

In equation 8, the vector $\boldsymbol{\theta}$, and variables *h, v, k, E,* $\boldsymbol{G}$, and LTE are as previously defined, the index *j* denotes the j-th TSD sensor, which is at a distance x_j from the TSD wheel, the variable c_i denotes the distance between the TSD wheel and the joint at the station where the i-th measurement was collected, and *n* denotes the length of the v_y profile (for measurements started 1.5m ahead of the joint to +1.0m after the joint, at 5cm resolution, $n = 51$). Also, μ and σ are the average and standard deviations of the TSD data and modeled v_y signals respectively. In the current implementation of equation 8, it was decided to not optimize $\boldsymbol{G}$ and assume $G = 0$ (Winkler foundations).

Figure 7 and Figure 8 show examples of matched v_y signals to simulated, noiseless, TSD data for the sensors at x = 210mm and x = 600mm, generated during *v_y-matcher*'s beta-testing stage for two sets of pavement parameters.

- **Simulated Example #1 [Figure 7]: E = 33.1 GPa, K = 3.3x10^7 N/m^3, LTE = 0.80**
- **Simulated Example #2 [Figure 8]: E = 39.3 GPa, K = 3.3x10^7 N/m^3, LTE = 0.80**
- **Remaining parameters (equal for both examples): h = 0.15m, G = 0, Load = 40 kN, p = 793 kPA, 2b = 0.50m, v = 0.20, v_x = 17.78 m/sec.**

It was found that *v_y-matcher* may match the input data to the v_y profile of any pavement case whose E/k ratio is close to that of the measured pavement and the pavement properties can be determined by scaling those of the matched v_y signal using the ratio of the v_y signal and TSD data.

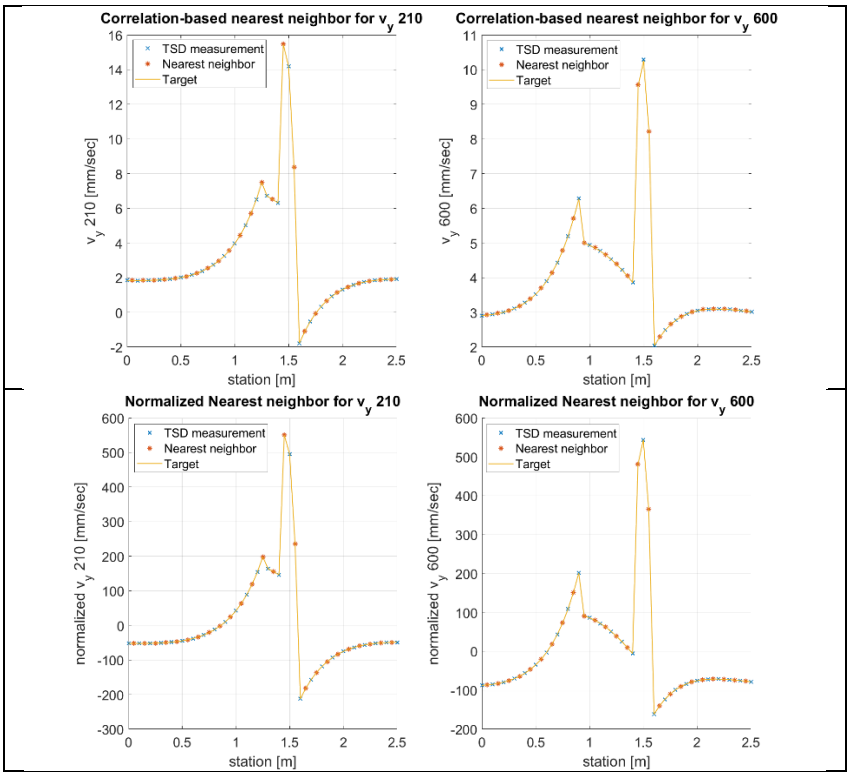

Figure 7: V_y-matcher's outcome for vy-210 and vy-600 on simulated example #1: v_y-matcher's *reported nearest neighbor* matched the target and the measurements. Top: Raw signals. Bottom: normalized signals.

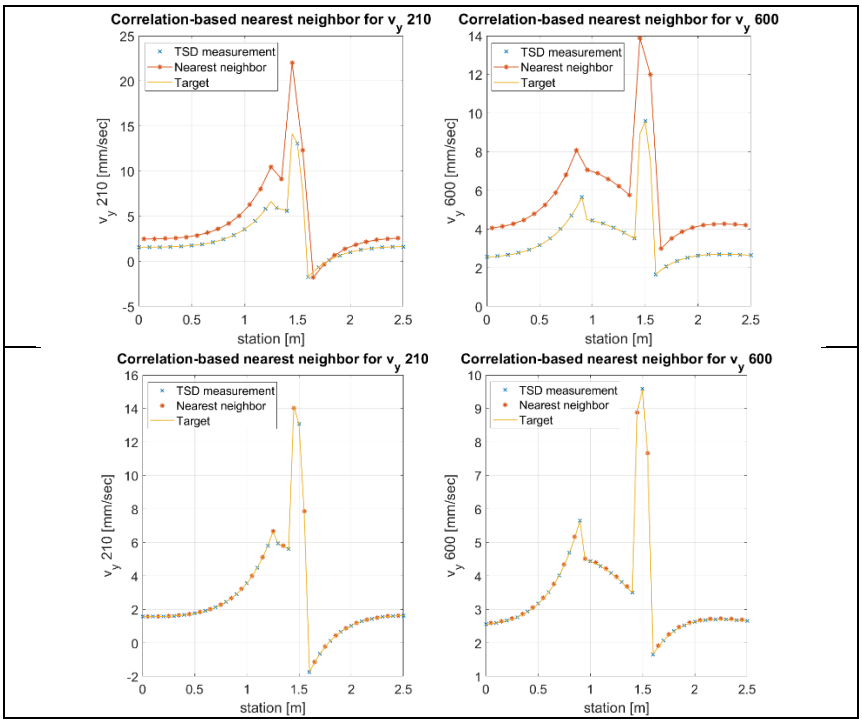

Figure 8: V_y-matcher's outcome for vy-210 and vy-600 on simulated example #2: Top: Raw signals (nearest neighbor mismatched the measurements). Bottom: Raw signals and matched neighbor after scaling, a match was attained.

As expected, the noise level in the TSD data affects the accuracy of determining the *E/k* and thus the *E* and *k* estimates may become less accurate. However, the noise has a smaller effect on the accuracy of determining the LTE, and in general, it can still be estimated within +/-5% of the target value. Figure 9, which is the correlation-vs-*E/k* plot for a simulated noisy case study with a known *target* (same parameters as Simulated Example #1), graphically shows how v_y signals from cases other than the target – even for LTE different than the target LTE – might correlate to the recovered measurements better than the target signal.

Consequently, the correlation-based *v_y-matcher* may correctly return the joint's LTE index and the *E/k* ratio for the surveyed section, provided that the input data is not extremely distorted by measurement noise. This becomes an issue when processing measurements from strong joints and/or very stiff pavements, for which the v_y signals are faint and more likely to be garbled by measurement noise; yet these joints hardly pose a concern to the pavement manager, because they boast good structural health. On the other hand, TSD data from weak concrete pavement sections can be reasonably processed with *v_y-matcher* and the pavement's structural parameters can be estimated somewhat reliably. Meanwhile, in any case, from the tested simulated studies, *v_y-matcher* should approximate the joint's LTE from noisy data within +/-5% of the target value.

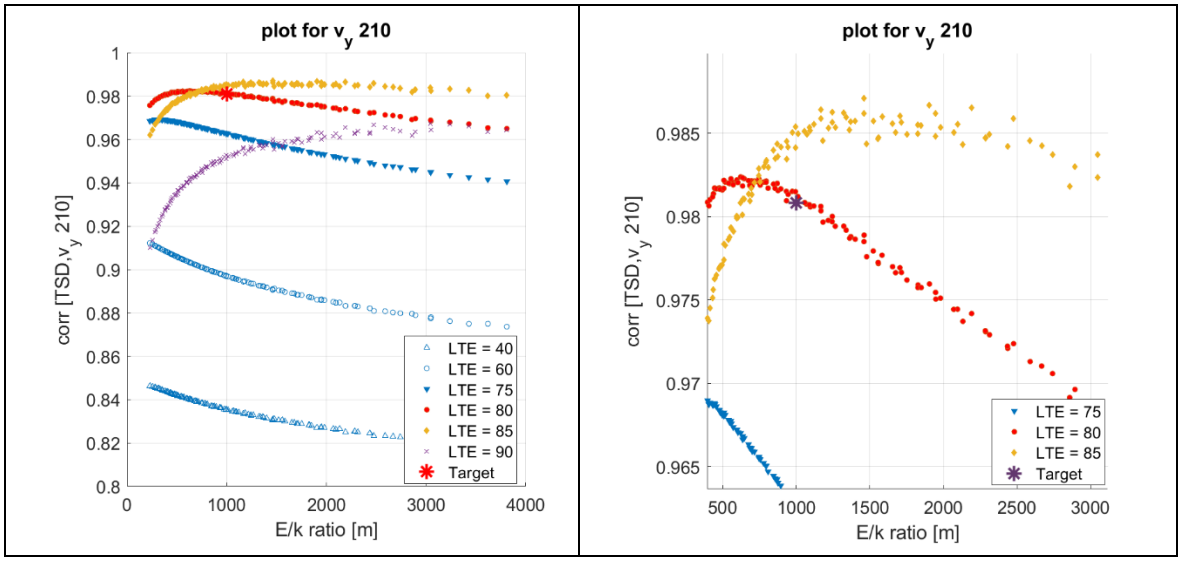

Figure 9: Correlation plot between a normalized denoised v_y profile [simulated] and multiple modeled v_y profiles vs E/k ratio, color-coded by LTE index. Left: Plots for multiple E/k and LTE cases. Right, sub-set of the LTE=0.75, 0.80, and 0.85 plot showing that multiple v_y profiles with E/k close to the ground truth correlate better to the input data than the target neighbor [Target: E/k = 1000, LTE = 0.80]

CHAPTER 4. References

Alavi, S.; LeCates, J. F.; & Tavares, M. P. (2008): *Falling Weight Deflectometer Usage.* (NCHRP Synthesis 381). Transportation Research Board. Washington, DC

Austroads (2016): *Specification for Pavement Deflection Measurement with a Traffic Speed Deflectometer (TSD) Device*. Austroads Test Method AG:AM/S006. Sydney, Australia.

Barman, M.; Roy, S.; Tiwari, A.; Burnham, T. (2021): *Performance Benefits of Fiber-reinforced Thin Concrete Pavement and Overlays. Final Report.* (Report MN/RC 2019-XX). Minnesota Department of Transportation. Office of Research & Innovation. June 2021.

Deep, P., Andersen, M. B., Rasmussen, S., Thom, N., Marradi, A., & Presti, D. L. (2020). Evaluation of Load transfer in rigid pavements by Rolling wheel deflectometer and Falling weight deflectometer. *Transportation Research Procedia, 45*, 376-383.

Flintsch, G. W., Katicha, S.W., Bryce, J., Ferne, B., Nell, S., & Diefenderfer, B. (2013): *Assessment of Continuous Pavement Deflection Measuring Technologies.* Second Strategic Highway Research Program (SHRP2) Report S2-R06F-RW-1, The National Academies, Washington, DC.

Hernandez, J. (2023): Back-calculation of rigid pavements from Traffic Speed Deflectometer Measurements. Article in Press. Transportation Research Record.

Hildebrand, G. & Rasmussen, S. (2002): Development of a high-speed deflectograph. Danish Road Institute Rep. 117. Road Directorate, Danish Road Institute. Roskilde, Denmark.

Horak, E. (2008). Benchmarking the structural condition of flexible pavements with deflection bowl parameters. *Journal of the South African Institution of Civil Engineering, 50*(2), 2-9.

Jendzurski, J. & Paulter, N. G. (2008): Calibration of Speed Enforcement Down-the-road radars. *Journal of Research of the National Institute of Standards and Technology. 114*, 137-148

Katicha, S. W., Flintsch, G., Bryce, J., & Ferne, B. (2014). Wavelet denoising of TSD deflection slope measurements for improved pavement structural evaluation. *Computer-Aided Civil and Infrastructure Engineering*, *29*(6), 399-415.

Katicha, S. W., Loulizi, A., Khoury, J. E., & Flintsch, G. W. (2017). Adaptive false discovery rate for wavelet denoising of pavement continuous deflection measurements. *Journal of computing in civil engineering*, *31*(2), 04016049.

Katicha, S. W., Flintsch, G. W., Shrestha, S., Scavone, M. (2021): *Overview of TSDD Technologies and Their Network- and Project-Level Applications.* TPF-5(385) Pavement Structural Evaluation with Traffic Speed Deflection Devices. Task 1. Virginia Tech Transportation Institute. Blacksburg, VA.

Khazanovich, L., K. Kosar, & H. Li (2021): *Evaluation of Long-Term Impacts of Early Opening of Concrete Pavements.* (Report NRRA202111). Minnesota Department of Transportation.

Krarup, J.; Rasmussen, S.; Aagaard, L.& Hjort, P. G. (2006): Output from the Greenwood Traffic Speed Deflectometer. *22nd ARRB Conference – Research into Practice.* Canberra, Australia.

Muller, W. B.; Roberts, J. (2013): Revised Approach to Assessing Traffic Speed Deflectometer Data and Field Validation of Deflection Bowl Predictions. *International Journal of Pavement Engineering 14*(4) 388-402.

Nielsen, C. P., & Jensen, K. (2021, November). Traffic speed deflectometer measurements at Copenhagen airport. In *Eleventh International Conference on the Bearing Capacity of Roads, Railways and Airfields, Volume 1* (pp. 458-465). CRC Press.

Nielsen, C. P., Nahoujy, M. R., & Jansen, D. (2023). Measuring Joint Movement on Rigid Pavements Using the Traffic Speed Deflectometer. *Journal of Transportation Engineering, Part B: Pavements, 149*(2), 04023002.

Phares, B. M.; Ceyland, H.; Souleyrette, R.; Smadi, O.; & Gopalakrishnan, K. (2008): *Development of a High-Speed Rigid Pavement Analyzer – Phase I Feasibility and Need Study.* CTRE Project 06-281 Report. Iowa State University. May 2008

Pierce, L. M., Bruinsma, J. E., Smith, K. D., Wade, M. J., Chatti, K., & Vandenbossche, J. (2017). *Using falling weight deflectometer data with mechanistic-empirical design and analysis, volume III: Guidelines for deflection testing, analysis, and interpretation.* (No. FHWA-HRT-16-011). United States. Federal Highway Administration.

Rada, G. R., Nazarian, S., Visintine, B. A., Siddharthan, R. V., & Thyagarajan, S. (2016). *Pavement structural evaluation at the network level.* (No. FHWA-HRT-15-074). Federal Highway Administration. Office of Infrastructure Research and Development.

Rohde, G. T. & Smith, R. E. (1991): *Determining Depth to Apparent Stiff Layer from FWD Data.* (FHWA/TX-91-1159-1). October 1991

Scavone, M. (2022): *Use of the Traffic Speed Deflectometer for Concrete and Composite Pavement Structural Health Assessment. A Big-Data-Based Approach Towards Concrete and Composite Pavement Management and Rehabilitation*. Ph. D. Dissertation. Virginia Tech. August 2022. Blacksburg, VA.

Scavone, M., Katicha, S. W., Flintsch, G. W., & Amarh, E. (2022). On the TSD deflection velocity measurements: a revision to the current state of the art and discussion over its applicability for concrete pavement assessment. *International Journal of Pavement Engineering,* 1-13.

Scavone, M., Katicha, S. W., Flintsch, G. W., & Amarh, E. (2023). *Estimating Load Transfer Efficiency for Jointed Pavements from TSD Deflection Velocity Measurements.* Transportation Research Record. DOI: 10.1177/03611981231171923.

Schmalzer, P; Rada, G & Miller, J. S. (2007): *Falling Weight Deflectometer (FWD) Testing and Analysis Guidelines Volume 1.* (FHWA-FLH-07-001) FHWA. Federal Lands Highway Division. October 2007

Ullidtz, P. *Pavement Analysis*. Elsevier, Amsterdam, 1987.

Van Cauwelaert, F. (2004). *Pavement design and evaluation. The required mathematics and its applications.* Federation of the Belgian Cement Industry, Brussels.

Van Deusen, D. A., Burnham, T. R., Dai, S., Geib, J., Hanson, C., Izevbekhai, B. I., ... & Worel, B. (2018). *Report on 2017 MnROAD Construction Activities.* (No. MN/RC 2018-16). Minnesota. Dept. of Transportation. Research Services & Library.

Appendix 1: How the TSD generates pavement surface v_y measurements

Note: This appendix is a review of a procedure published by Scavone et al. (2022)

The TSD collects pavement surface deflection velocity [v_y] data from Doppler Laser Vibrometers mounted along its longitudinal direction, at different distances from its rear axle. Most of these sensors measure the pavement surface velocity relative to the TSD for points on the pavement within the TSD axle's deflection basin, whereas one additional sensor located far away from the rear axle (*the reference sensor*) measures the relative velocity of the pavement surface at a location deemed as undeflected (**Hildebrand and Rasmussen, 2022; Krarup et al., 2006**). This appendix presents the mathematical procedure to determine v_y for a location within the deflection basin from the measurement from a Doppler Laser Vibrometer targeted at it plus the measurement from the *reference sensor*. The formulae presented herein were originally published by Scavone et al. (2022).

Figure 10 represents the featured two-sensor arrangement. Sensor 1 refers to the Doppler Sensor aimed at a point within the deflection basin [point 1], and Sensor 0 is *the reference sensor,* aimed at point 0. Sensors 0 and 1 are skewed at angles α_0 and α_1 from the vertical direction [angles θ_0 and θ_1 are complementary to α_0 and α_1]; the TSD (and thus sensors 0 and 1) are traveling horizontally with speed v_x. Sensor 0's and Sensor 1's measurements are denoted M_0 and M_1 respectively and represent the velocity of points 0 and 1 on the pavement surface relative to the TSD. As such, point 0's relative velocity to Sensor 0 is v_x horizontally and no vertical component, and point 1's velocity (vector v_1 in Figure 10) has both a horizontal component equal to v_x plus a vertical component equal to v_y, β is the angle formed by v_1 and the horizontal direction.

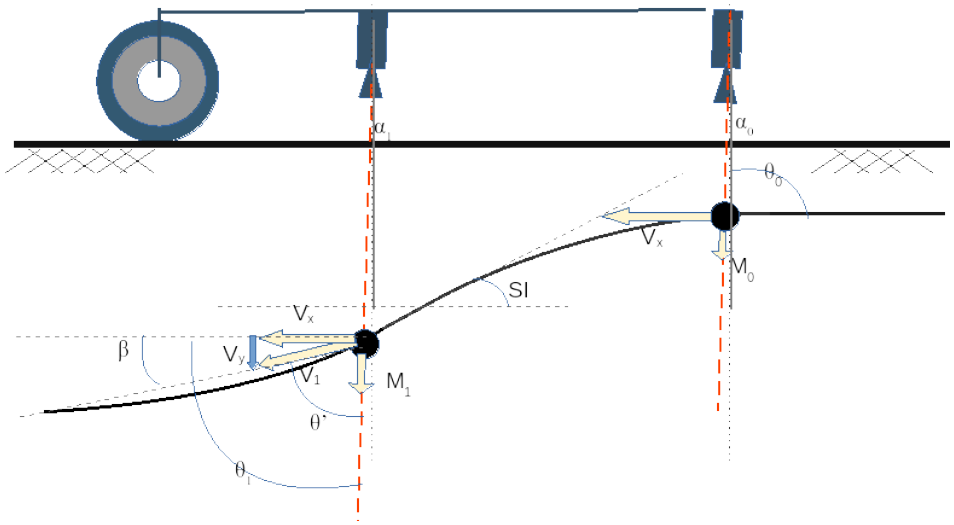

Figure 10: Measurement of pavement's v_y at a point within the deflection basin from two TSD measurements. Definition of variables. From Scavone et al. (2022)

Measurement M_0 is a projection of v_x on the direction of sensor 0's beam, thus:

$$M_0 = v_x cos(90deg - \alpha_0) = v_x sin(\alpha_0)$$
$$v_x = \frac{M_0}{sin(\alpha_0)} \quad (9)$$

Similarly, measurement M_1 would collect a projection of v_1 over the direction of its laser beam, thus:

$$M_1 = v_1 cos(\theta') \quad (10)$$

Since angle θ' is equal to θ_1 minus β it holds that:

$$M_1 = v_1 cos(\theta_1 - \beta) \quad (11)$$

By replacing the *cosine of a difference* in equation 11 by the cosine identity: cos(a – b) = cos(a)cos(b) + sin(a)sin(b) leads to:

$$M_1 = v_1[cos(\theta_1)cos(\beta) + sin(\theta_1)sin(\beta)] \quad (12)$$

Meanwhile, the horizontal component of v_1 is v_x, and so:

$$v_x = v_1 cos(\beta) \quad (13)$$

Merging the result from equation 13 into equation 12 gives:

$$M_1 = \frac{v_x}{cos(\beta)}[cos(\theta_1)cos(\beta) + sin(\theta_1)sin(\beta)]$$
then:
$$M_1 = v_x[cos(\theta_1) + sin(\theta_1)tan(\beta)] \quad (14)$$

Moreover, by applying to the relationship between θ_1 and α_1 (complementary angles) and rearranging terms in equation 14 leads to:

$$M_1 = v_x[sin(\alpha_1) + cos(\alpha_1)tan(\beta)] \quad (15)$$
$$M_1 - v_x sin(\alpha_1) = v_x cos(\alpha_1)tan(\beta)$$
then:
$$\frac{M_1 - v_x sin(\alpha_1)}{v_x cos(\alpha_1)} = tan(\beta) \quad (16)$$

At this point, v_x can be substituted in equation 16 by its estimate from measurement M_0 (equation 9). This leads to an expression to estimate angle β from M_1 and M_0:

$$\frac{M_1 - M_0 \frac{sin(\alpha_1)}{sin(\alpha_0)}}{v_x cos(\alpha_1)} = tan(\beta) \quad (17)$$

Since $v_y = v_1 sin(\beta) = v_x tan(\beta)$, then v_y can be solved as a function of M_1 and M_0 by rearranging equation 17.

$$\frac{M_1 - M_0 \frac{sin(\alpha_1)}{sin(\alpha_0)}}{cos(\alpha_1)} = v_y \tag{18}$$

Finally, the TSD's Doppler laser sensors are customarily skewed from the vertical direction only very slightly, thus angles α_1 and α_0 are small (about 2 degrees), and so $\cos(\alpha_1) \sim \cos(\alpha_0) \sim 1$. This simplifies equations 17 and 18 as follows [the sine terms cannot be simplified, however]:

$$\frac{M_1 - M_0 \frac{sin(\alpha_1)}{sin(\alpha_0)}}{v_x} = tan(\beta) \tag{19}$$

$$M_1 - M_0 \frac{sin(\alpha_1)}{sin(\alpha_0)} = v_y \tag{20}$$

Equation 18 **also shows how crucial it is to know the angles α_0 and α_1 to ensure accurate v_y measurements, inexact angle measurements would lead to erroneous v_y data.** Moreover, inexact approximations of α_1 and α_0 may even make the v_y measurement null.

Appendix 2: Discussion on the relationship between V_y and deflection slope

Note: This appendix is a review of findings by Scavone et al. (2022)

Introduction:

A generally accepted premise of TSD data processing is that the slope of the deflection basin [*Sl*] at a given point on the pavement surface can be determined from the TSD's v_y data measurement and travel speed v_x as per the following relationship (Hildebrand and Rasmussen, 2002; Krarup et al., 2006):

$$Sl = \frac{V_y}{V_x} \tag{21}$$

Throughout the multiple research efforts concerning TSD operation and data handling carried out to date, the relationship in equation 21 has been assumed as an immutable hypothesis, researchers then proposed different processing techniques to integrate the *Sl* estimates into measurements of the depth of the deflection basin – for a review of those procedures, refer to Katicha et al., 2021; Scavone 2022.

However, when inspecting the TSD data from a jointed pavement with known properties and comparing it against simulated responses from linear-elastic slab theory (Van Cauwelaert, 2004), a discrepancy was found: at locations nearby the joint, the simulated deflection slope for points ahead of the TSD wheel, which are at all times descending into the deflection bowl, changes sign. Such a behavior cannot be explained by the relationship in equation 21, thus forcing a revision. Figure 11 illustrates this discrepancy for a sample of real 5cm resolution TSD deflection slope estimates from the MnROAD test track. Such slope estimates were computed with equation 21, meaning these are actually scaled v_y measurements. The figure shows that the slope estimates do not match the simulated slope data, but they do resemble the simulated pavement surface v_y.

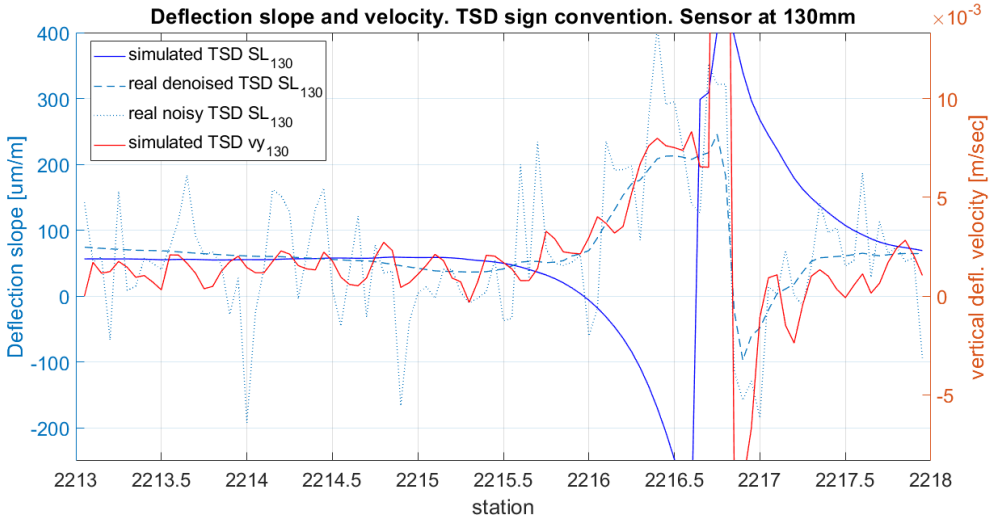

Figure 11: Simulated slope and vertical surface velocity signals against a TSD measurement – Sensor at 130mm ahead from the TSD wheel.

Statement: Relationship between v_y and deflection basin slope and validity of the slope-v_y direct relationship

The pavement surface point's deflection velocity [v_y] is constituted by two components:

- One component relates to the rate of change in shape of the deflection basin produced by the TSD load applied on the pavement.
- The second component is due to the horizontal movement of the deflection basin, this term relates v_y to the slope of the basin *S* and the TSD travel speed v_x

When the deflection basin produced by the TSD load is *stationary* (that is, it keeps constant shape throughout the many locations where the TSD measurements take place), only then equation 21 **is valid.**

Proof (Scavone et al., 2022)

The pavement deflection function *w* depends on its location (*x*) and the pavement structure properties (summarized as *M,* which are a function of the location *x* as well). Since the TSD travels horizontally along the pavement, *x* is, in turn, a function of the time *t*.

$$w = w\left(x(t), M\left(x(t)\right)\right) \tag{22}$$

The pavement surface deflection velocity v_y for a given point is the total derivative of *w* over time. Thus, differentiating w and applying the *chain rule:*

$$v_y = \frac{dw}{dt} = \frac{\partial w}{\partial x}\frac{\partial x}{\partial t} + \frac{\partial w}{\partial M}\frac{\partial M}{\partial x}\frac{\partial x}{\partial t} \tag{23}$$

The second term of the *chain rule* could be simplified by defining function *w** as the component of *w* that only depends on the pavement properties. Rewriting equation 23 gives:

$$v_y = \frac{\partial w}{\partial x}\frac{\partial x}{\partial t} + \frac{\partial w^*}{\partial t} \tag{24}$$

Noticing that $v_x = \partial x/\partial t$ (because coordinate x moves with the TSD) and the slope of the deflection bowl $S = \partial w/\partial x$ (by definition), we have that:

$$\frac{\partial w}{\partial x}\frac{\partial x}{\partial t} = S v_x \tag{25}$$

Then, combining the results from equations 24 and 25**:**

$$v_y = S v_x + \frac{\partial w^*}{\partial t} \tag{26}$$

Equation 26 thus states that v_y is made of two main elements: a term (*the partial derivative term*) that relates to how the deflection basin changes shape because of changes in pavement properties (layer thickness, material properties, discontinuities in the pavement structure), plus the *slope term*, that is due to the fact that the TSD's deflection bowl is moving.

It can also be observed that the relationship in equation 21 is a particular case of equation 26 that is valid **only** if the *partial derivative term* is zero (or is quantitatively negligible compared to the *slope term*). This implies that equation 21 only holds for homogeneous stretches of pavement, that is, segments that have constant material properties are free of events that may alter the shape of the moving TSD deflection basin.

Proof concluded.

Geometric interpretation:

Equation 21 also has a geometric interpretation concerning the relative velocity vector v_1 for a point on the pavement surface that is within the deflection basin (refer to Appendix 1). Recalling that β is the angle of v_1 with respect to the horizontal line (Figure 10), then:

$$Sl = tan(\beta) = \frac{V_y}{V_x} \tag{27}$$

This result means that when the TSD deflection basin is *stationary,* vector v_1 is parallel to the deflection bowl slope, meaning that, relative to the TSD, points on the pavement surface *fall down the slope the bowl.*

Alternative *concept proof*

Note: The following is an alternative derivation of the non-direct relationship between deflection slope and v_y (equation 26) that, while lacking the rigor of the calculus-based proof, contributes to understanding the two terms that compose v_y.

A v_y measurement is a measurement of the velocity a given point on the pavement structure descends (difference between two surface elevation values for a point at a given station at different moments in time). Meanwhile, a *deflection slope measurement* is a measurement that represents the difference in elevation of two points at different stations but at the same moment in time.

Consider the deflection bowls from the TSD wheel at times t_0 and $t_1 = t_0 + \Delta t$ (**for an increment Δt small enough that v_y for a given point in the pavement surface may remain constant**). The TSD wheel is located at station $x = c_0$ at time t_0 and at station $x = c_1$ at time t_1. The TSD moves with horizontal speed v_x. Thus, it is immediate that $x_1 = x_0 + v_x \times \Delta t$, and in particular, $c_1 = c_0 + v_x \times \Delta t$.

The deflection basins for each timestamp are $w(z,t_0)$ and $w(z, t_1)$ respectively, where z is a coordinate that is moving with the TSD and centered at the TSD wheel centerline: at $t = t_0$, $z = 0$ corresponds with $x = c_0$, and at $t = t_1$, $z = 0$ corresponds to $x = c_1$). These variables are shown in Figure 6.

Consider now the deflection at a point located at a distance z from the TSD wheel (a distance from the TSD wheel where a Doppler sensor is located). At time t_0, its station is $x_0 = c_0 + z$, and at time t_1, its station is $x_1 = c_1 + z$. **Thus, the TSD sensor would gather data [v_y] for the point at station x_0 at time t_0 and for the point at station x_1 at time t_1**.

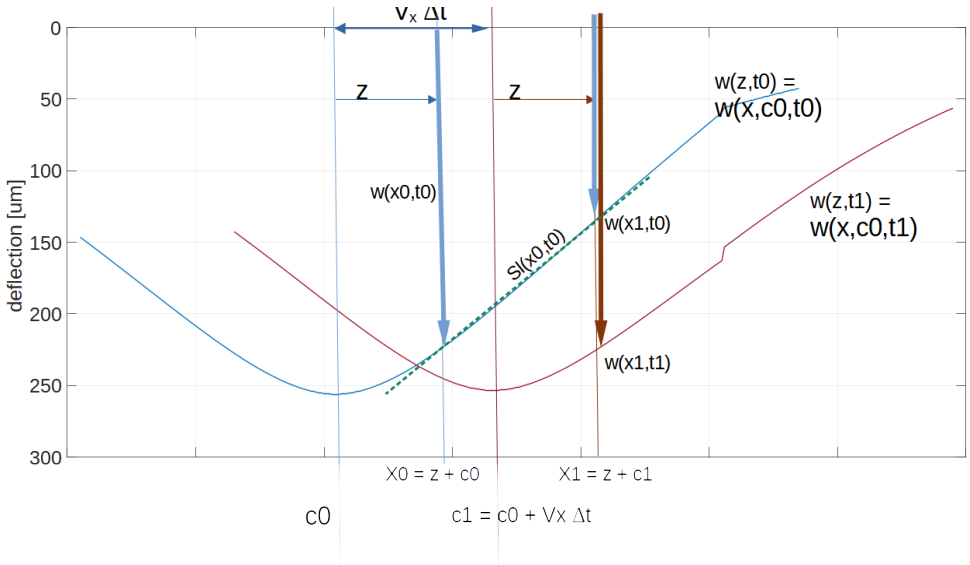

Figure 12: Definition of variables used in proof of concept. Deflection bowls for time t_0 and t_1, TSD wheel located at stations c_0 and c_1 respectively.

Approximate the deflection slope of the basin $w(z,t_0)$ for the points at station x_0 and x_1 (Slt_0)) as a finite difference using the deflections at x_0 and x_1 and time t_0

$$Sl(t_0) = \frac{\Delta w(z,t)|_{x_0}}{\Delta x} = \frac{w(x_1,t_0) - w(x_0,t_0)}{x_1 - x_0} \tag{28}$$

Knowing that $x_1 = x_0 + v_x \times \Delta t$, it holds:

$$Sl(x_0) = \frac{\Delta w(x,t)}{\Delta x} = \frac{w(x_1,t_0) - w(x_0,t_0)}{v_x \Delta t} \tag{29}$$

As stated before, the TSD would collect data about point x_0 at time t_0, but none about point x_1 at t_0 (the Doppler vibrometer will only sense point x_1 at time t_1). However, $w(x_1,t_0)$ could be approximated from $w(x_1,t_1)$ and $v_y(x_1)$:

$$v_y(x_1,t_1) = v_y(x_1,t_0) = v_y(x_1) = \frac{w(x_1,t_1) - w(x_1,t_0)}{\Delta t}$$
$$\text{then:}$$
$$w(x_1,t_0) = w(x_1,t_1) - v_y \times \Delta t \tag{30}$$

Equation 30 assumes that the v_y is constant between times t_0 and t_1, hence the original assumption of a small interval Δt.

Merging equations 28 and 30 and rearranging:

$$Sl(t_0) = \frac{w(x_1,t_1) - v_y \times \Delta t - w(x_0,t_0)}{v_x \Delta t} \tag{31}$$

$$Sl(t_0) = \frac{1}{v_x} \times \frac{w(x_1,t_1) - w(x_0,t_0)}{\Delta t} - \frac{v_y}{v_x} \tag{32}$$

Now, if we recall that the x_0, x_1 within function *w* are actually functions of c_0, c_1, and the moving coordinate *z,* equation 32 becomes:

$$Sl(t_0) = \frac{1}{v_x} \times \frac{w(c_1, z) - w(c_0, z)}{\Delta t} - \frac{v_y}{v_x} \tag{33}$$

Rearranging terms and relating c_1 and c_0:

$$v_y = Sl(t_0) \times v_x + \frac{w(c_0 + \Delta t, z) - w(c_0, z)}{\Delta t} \tag{34}$$

Equation 34 (an *approximation* to equation 26) shows that v_y and the deflection basin slope are not directly related: In fact, v_y is made of the *slope term* plus a term that encodes the rate at which the deflection basin ($w(z)$) changes shape, regardless of the fact that the TSD's deflection bowl may also be moving – even a stopped TSD that applies a variable load on the pavement would force the pavement surface move up and down, and that movement would be encoded in the second right-hand term in equation 8.

Consequently, equation 34 shows that v_y and Sl are directly related (equation 21) only if the second right-hand-side term is zero, which occurs only if the deflection basin does not change shape.

Appendix 3: A slab-theory-based mathematical model for the deflection of a jointed concrete pavement

Note: This appendix is an abridged review, based on Scavone (2022), of the closed-form solutions to the deflection function for a jointed concrete slab on a Pasternak foundation, as solved by Van Cauwelaert (2004).

Slab theory approach

Van Cauwelaert (2004) solved the mathematical expression for a linear elastic slab-on-ground problem as shown in Figure 13. The pavement structure is supposed a pair of semi-infinite linear elastic concrete slabs with Young's modulus *E*, and Poisson's coefficient ν, and the slab thickness is *h*. Both slabs rest on a Pasternak foundation, which is a Winkler foundation capable of also withstanding shear stress – the foundation is characterized by its modulus of subgrade reaction *k* and a shear strength per unit length modulus **G**[3]**.** One of the slabs receives a uniformly distributed load, pressure *p*, spread over a rectangular area of dimensions *2a* by *2b*; the transverse joint is located at a distance *c* from the center of the load and is characterized by its deflection-ratio-based LTE index (Alavi et al., 2008; Pierce et al., 2017).

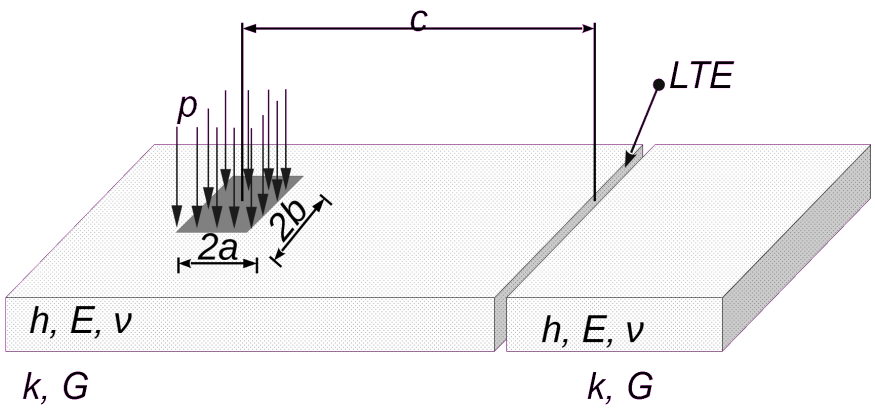

Figure 13: Definition of the jointed-slabs-on-ground problem.

The solution to the deflection basin that occurs in response to this load has a closed-form solution: It is a combination of the solution for an infinitely large continuous slab on ground, plus additional terms that account for the presence of the transverse joint. Van Cauwelaert (2004) states separate expressions for the loaded and unloaded slabs (equation 35).

$$\begin{aligned} w_L(x,y) &= w(x,y) + A \times w_A(x,y) + B \times w_B(x,y) \\ w_{UL}(x,y) &= C \times w_C(x,y) + D \times w_D(x,y) \end{aligned} \tag{35}$$

Note: Coordinate x is along the direction perpendicular to the transverse joint, and coordinate y is parallel to the transverse joint. The origin of coordinates is at the center of the applied load.

[3]A Winkler (dense liquid) foundation corresponds to the **G = 0** case.

Each of the terms in equation 35 is an infinite series over a dummy variable, the constants A, B, C, and D are solved from the boundary conditions imposed by the transverse joint for each value of the dummy variable as well – see equations 54 to 57.

Van Cauwelaert (2004) expresses the solutions to w_L and w_{UL} in terms of the following parameters: Westergaard's *radius of relative Stiffness [l],* the slab's *flexural rigidity,* and parameter *g,* which is somewhat similar to the *E/k* ratio but relating the slab's stiffness and the subgrade's shear strength.

$$l = \left[\frac{Eh^3}{12(1-\nu)^2 k}\right]^{1/4} \tag{36}$$

$$D = \left[\frac{Eh^3}{12(1-\nu)^2}\right] = k \times l^4 \tag{37}$$

$$g = \frac{Gl^2}{2D} = \frac{G}{2\sqrt{kD}} \tag{38}$$

Infinite slab component

The infinite slab component has different expressions for points located within and outside of the load's footprint area (Van Cauwelaert, 2004). Plus, these formulae also vary with the value of parameter *g*.

- Case $g < 1$ (includes Winkler foundation case $g = 0$)

for x $\geq a$

$$w(x,y) = \frac{p}{\pi k}\frac{1}{\sqrt{1-g^2}}\int_0^\infty w_3(y,s) \times [w_4(x,s) - w_5(x,s)]\, ds$$

where:

$$w_3(y,s) = \frac{cos(sy/l)sin(sb/l)}{s(s^4 + 2gs^2 + 1)}$$

$$w_4(x,s) = \frac{e^{-(x-1)\alpha/l}}{\sqrt{1-g^2}}\left[\sqrt{1-g^2}cos[(x-a)\,\beta/l] + (s^2+g)sin[(x-a)\,\beta/l]\right] \tag{39}$$

$$w_5(x,s) = \frac{e^{(x+a)\alpha/l}}{\sqrt{1-g^2}}\left[\sqrt{1-g^2}cos[(x+a)\,\beta/l] + (s^2+g)sin[(x+a)\,\beta/l]\right]$$

for x $< a$

$$w(x,y) = \frac{p}{\pi k}\frac{1}{\sqrt{1-g^2}}\int_0^\infty w_3(y,s) \times [2 - w_1(x,s) - w_2(x,s)]\, ds$$

where:

$$w_3(y,s) = \frac{cos(sy/l)sin(sb/l)}{s(s^4 + 2gs^2 + 1)}$$

$$w_1(x,s) = \frac{e^{-(a-x)\alpha/l}}{\sqrt{1-g^2}}\left[\sqrt{1-g^2}cos[(a-x)\,\beta/l] + (s^2+g)sin[(a-x)\,\beta/l]\right] \tag{40}$$

$$w_2(x,s) = \frac{e^{-(a+x)\alpha/l}}{\sqrt{1-g^2}}\left[\sqrt{1-g^2}cos[(a+x)\,\beta/l] + (s^2+g)sin[(a+x)\,\beta/l]\right]$$

Where the coefficients α and β are:

$$\alpha^2 = \frac{1}{2}\left[\sqrt{(s^2+g)^2+1-g^2} + (s^2+g)\right]$$
$$\beta^2 = \frac{1}{2}\left[\sqrt{(s^2+g)^2+1-g^2} - (s^2+g)\right] \quad (41)$$

- Case g > 1

$$\text{for x } \geq a$$
$$w(x,y) = \frac{p}{2\pi k}\frac{1}{\sqrt{g^2-1}}\int_0^\infty w_3(y,s) \times [w_4(x,s) - w_5(x,s)]\, ds$$
$$\text{where:}$$
$$w_3(y,s) = \frac{cos(sy/l)sin(sb/l)}{s}$$
$$w_4(x,s) = \frac{e^{-(x-a)z_2/l} - e^{-(x+a)z_2/l}}{z_2^2} \quad (42)$$
$$w_5(x,s) = \frac{e^{-(x-a)z_1/l} - e^{-(x+a)z_1/l}}{z_1^2}$$

$$\text{for x} < a$$
$$w(x,y) = \frac{p}{2\pi k}\frac{1}{\sqrt{g^2-1}}\int_0^\infty w_3(y,s) \times [w_1(x,s) - w_2(x,s)]\, ds$$
$$\text{where:}$$
$$w_3(y,s) = \frac{cos(sy/l)sin(sb/l)}{s}$$
$$w_1(x,s) = \frac{2 - e^{-(a-x)z_2/l} - e^{-(a+x)z_2/l}}{z_2^2} \quad (43)$$
$$w_2(x,s) = \frac{2 - e^{-(a-x)z_1/l} - e^{-(a+x)z_1/l}}{z_1^2}$$

Where the coefficients z_1 and z_2 are:

$$z_1^2 = (s^2+g) + \sqrt{g^2-1}$$
$$z_2^2 = (s^2+g) - \sqrt{g^2-1} \quad (44)$$

- Case g = 1

$$\text{for x } \geq a$$

$$w(x,y) = \frac{p}{2\pi k}\frac{1}{\sqrt{g^2-1}}\int_0^\infty w_3(y,s) \times [w_4(x,s) - w_5(x,s)]\, ds$$

$$\text{where:}$$

$$w_3(y,s) = \frac{cos(sy/l)sin(sb/l)}{s(s^2+1)^2}$$

$$w_4(x,s) = e^{-(x-a)z/l}\left[2 + \sqrt{1+s^2}\,(x-a)/l\right] \tag{45}$$

$$w_5(x,s) = e^{-(x+a)z/l}\left[2 + \sqrt{1+s^2}\,(x+a)/l\right]$$

$$\text{for x} < a$$

$$w(x,y) = \frac{p}{2\pi k}\frac{1}{\sqrt{g^2-1}}\int_0^\infty w_3(y,s) \times [4 - w_1(x,s) - w_2(x,s)]\, ds$$

$$\text{where:}$$

$$w_3(y,s) = \frac{cos(sy/l)sin(sb/l)}{s(s^2+1)^2}$$

$$w_1(x,s) = (x,s) = e^{-(a-x)z/l}\left[2 + \sqrt{1+s^2}\,(a-x)/l\right] \tag{46}$$

$$w_2(x,s) = (x,s) = e^{-(a+x)z/l}\left[2 + \sqrt{1+s^2}\,(a+x)/l\right]$$

Where the coefficient z is:

$$z^2 = (s^2+1) \tag{47}$$

Additional components for the jointed slab case

Following are the expressions for terms w_A, w_B, w_C, and w_D. As with the case of the infinite slab component, these also depend on the value of g. Van Cauwelaert (2004) warns that these equations are valid only for the case of a transverse joint located to the right of the load. The sign convention used in the following equations may change when modeling the response of the pavement once the load is on the right-hand-side slab.

- Case g < 1 (includes Winkler foundation case g = 0)

$$w_A(x,y) = \frac{p}{\pi k}\frac{1}{\sqrt{1-g^2}}\int_0^\infty \left[[A(s)cos(\beta\, x/l)]e^{\alpha x/l} \times \frac{cos(sy/l)sin(sb/l)}{s}\right] ds$$

$$w_B(x,y) = \frac{p}{\pi k}\frac{1}{\sqrt{1-g^2}}\int_0^\infty \left[[B(s)sin(\beta\, x/l)]e^{\alpha x/l} \times \frac{cos(sy/l)sin(sb/l)}{s}\right] ds \tag{48}$$

$$w_C(x,y) = \frac{p}{\pi k}\frac{1}{\sqrt{1-g^2}}\int_0^\infty \left[[C(s)cos(\beta\, x/l)]e^{-\alpha x/l} \times \frac{cos(sy/l)sin(sb/l)}{s}\right] ds$$

$$w_D(x,y) = \frac{p}{\pi k}\frac{1}{\sqrt{1-g^2}}\int_0^\infty \left[[D(s)sin(\beta\, x/l)]e^{-\alpha x/l} \times \frac{cos(sy/l)sin(sb/l)}{s}\right] ds \tag{49}$$

In equations 48 and 49, α and β are as per equation 41.

- Case g > 1

$$w_A(x,y) = \frac{p}{2\pi k}\frac{1}{\sqrt{g^2-1}}\int_0^\infty \left[A(s)e^{z_1 x/l} \times \frac{cos(sy/l)sin(sb/l)}{s}\right] ds$$
$$w_B(x,y) = \frac{p}{2\pi k}\frac{1}{\sqrt{g^2-1}}\int_0^\infty \left[B(s)e^{z_2 x/l} \times \frac{cos(sy/l)sin(sb/l)}{s}\right] ds \quad (50)$$

$$w_C(x,y) = \frac{p}{2\pi k}\frac{1}{\sqrt{g^2-1}}\int_0^\infty \left[C(s)e^{-z_1 x/l} \times \frac{cos(sy/l)sin(sb/l)}{s}\right] ds$$
$$w_D(x,y) = \frac{p}{2\pi k}\frac{1}{\sqrt{g^2-1}}\int_0^\infty \left[D(s)e^{-z_2 x/l} \times \frac{cos(sy/l)sin(sb/l)}{s}\right] ds \quad (51)$$

In equations 50 and 51, z_1 and z_2 are as per equation 44.

- Case g = 1

$$w_A(x,y) = \frac{p}{2\pi k}\int_0^\infty \left[A(s)e^{xz/l} \times \frac{cos(sy/l)sin(sb/l)}{s}\right] ds$$
$$w_B(x,y) = \frac{p}{2\pi k}\int_0^\infty \left[\frac{x}{l}B(s)e^{xz/l} \times \frac{cos(sy/l)sin(sb/l)}{s}\right] ds \quad (52)$$

$$w_C(x,y) = \frac{p}{2\pi k}\int_0^\infty \left[C(s)e^{-xz/l} \times \frac{cos(sy/l)sin(sb/l)}{s}\right] ds$$
$$w_C(x,y) = \frac{p}{2\pi k}\int_0^\infty \left[\frac{x}{l}D(s)e^{-xz/l} \times \frac{cos(sy/l)sin(sb/l)}{s}\right] ds \quad (53)$$

In equations 52 and 53, z is as per equation 47.

Boundary conditions imposed by the joint.

Equations 48 to 53 were stated in terms of four parameters A, B, C, D (s) that allow for the final deflection basin solution (equation 35) to be composed. The transverse joint imposes four boundary conditions, which provide the equations needed to compute these unknowns:

- Load transfer efficiency LTE = δ at x = c and any value of y

$$\delta \times \left(w(s) + A(s)w_A(s) + B(s)w_B(s)\right)\Big|_{x=c} = C(s)w_C(s) + D(s)w_D(s)|_{x=c} \quad (54)$$

- Cancellation of bending moments at the edge of the loaded slab (x = c)

$$\left(\frac{\partial^2}{\partial x^2} + \nu\frac{\partial^2}{\partial y^2}\right)\left(w(s) + A(s)w_A(s) + B(s)w_B(s)\right)\Big|_{x=c} = 0 \quad (55)$$

- Cancellation of bending moments at the edge of the unloaded slab (x = c)

$$\left(\frac{\partial^2}{\partial x^2} + \nu\frac{\partial^2}{\partial y^2}\right)\left(C(s)w_C(s) + D(s)w_D(s)\right)\Big|_{x=c} = 0 \quad (56)$$

- Equality of shear forces in the subgrade material (x = c)

$$\left(\frac{\partial^3}{\partial x^3}+(2-\nu)\frac{\partial^3}{\partial x\partial y^2}-\frac{2g}{l^2}\right)\left(w(s)+A(s)w_A(s)+B(s)w_B(s)\right)\Big|_{x=c}=\ldots$$
$$\ldots=\left(\frac{\partial^3}{\partial x^3}+(2-\nu)\frac{\partial^3}{\partial x\partial y^2}-\frac{2g}{l^2}\right)\left(C(s)w_C(s)+D(s)w_D(s)\right)\Big|_{x=c} \quad (57)$$

Equations 54 through 57 make a 4-by-4 linear system that can be solved for A, B, C, D for each value of the dummy variable s. The terms w(s), $w_A(s)$, $w_B(s)$, $w_C(s)$, $w_D(s)$ are the expressions within the integral for each of the variables w, w_A, w_B, w_C, and w_D (as per equations 39 to 53).

In practice, stating the system of equations 54 through 57 involves performing several partial derivatives of the functions w, w_A, w_B, w_C, and w_D. These derivatives can be computed numerically by finite differences (Scavone, 2022).

Solving the case of a load stepping over the joint by superposition.

Van Cauwelaert's (2004) solution to the slab-on-ground problem does not include the case of a load simultaneously distributed over both slabs. However, the underlying assumption of linearity of the concrete slab and the subgrade allows solving this case by superposition of two problems, one component corresponding to the portion of the load on the left-hand-side slab and the other component representing the portion of the load on the right-hand-side slab (figure 14). For each sub-problem, the dimensions of the applied load and the variable *c* – the distance between the load center and the joint – must be corrected accordingly.

4.1.1. Computing deflection slope and velocity from the linear elastic model

The deflection slope and deflection velocity [v_y] signals of the TSD can be simulated from the slab-on-ground model. Computing the deflection slope from the deflection basin is easy, for it only involves deriving w_L or w_{UL} (equation 58):

$$\text{for x} < \text{c:}\quad slope(x,y)=\frac{\partial}{\partial x}w_L(x,y)$$
$$\text{for x} \geq \text{c:}\quad slope(x,y)=\frac{\partial}{\partial x}w_{UL}(x,y) \quad (58)$$

These derivatives can be solved numerically by finite differences (Scavone, 2022).

However, computing v_y for a given point on the pavement surface from two displaced deflection basins is a more delicate procedure since the amount of horizontal movement of the deflection basins must be considered and because the slab-on-ground problem must be cast appropriately for each location of the deflection bowl.

Scavone (2022) suggests the following formula to estimate v_y from two bowls that are separated by a distance $v_x\,\Delta t$:

$$\text{for x} < \text{c:}\quad v_y(x,y)=\frac{w_L(x-v_x\Delta t,y,c-v_x\Delta t)-w_L(x,y,c)}{\Delta t}$$
$$\text{for x} \geq \text{c:}\quad v_y(x,y)=\frac{w_{UL}(x-v_x\Delta t,y,c-v_x\Delta t)-w_{UL}(x,y,c)}{\Delta t} \quad (59)$$

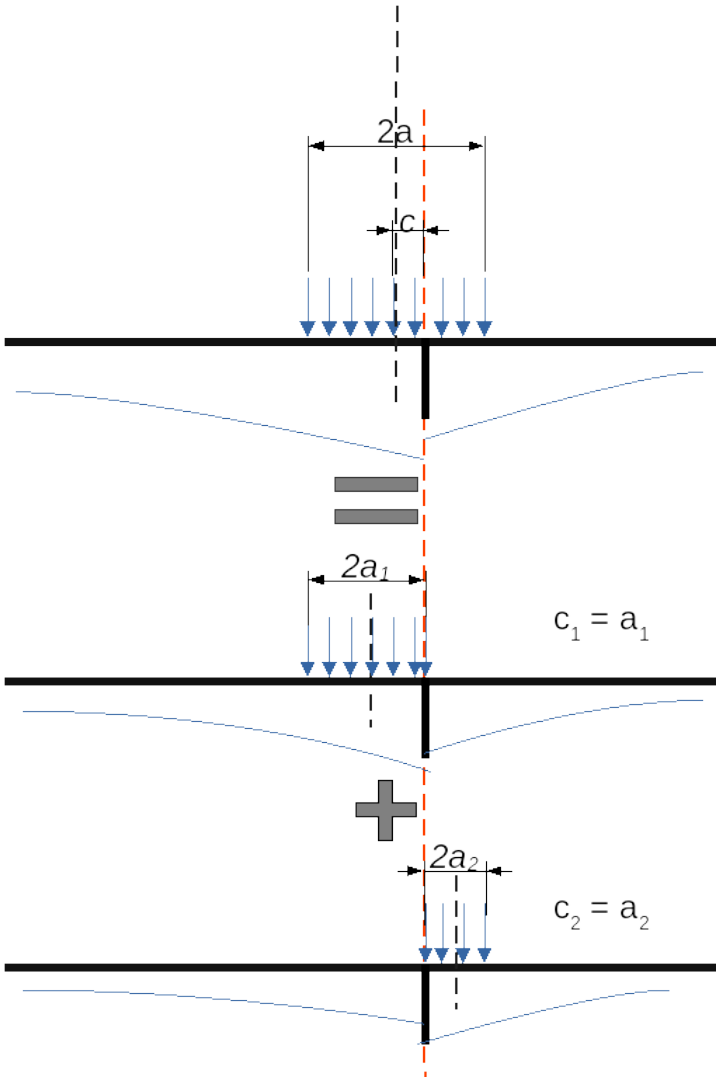

Figure 14: Treating the case of the load invading the joint as two separate problems and applying superposition to attain the final solution.